Artificial Intelligence Based Vector Control of Induction Generator without Speed Sensor for Use in Wind Energy Conversion System

Boris Dumnic*, Bane Popadic*, Dragan Milicevic*, Vladimir Katic*, Djura Oros*

*Department of Power, Electronics and Communication Engineering, Faculty of Technical Sciences, University of Novi Sad, Novi Sad, Serbia

dumnic@uns.ac.rs, banep@uns.ac.rs, milicevd@uns.ac.rs, katav@uns.ac.rs, orosd@uns.ac.rs

‡Boris Dumnic; Trg Dositeja Obradovica no. 6, 21000 Novi Sad, Serbia, Tel: +381 21 485 2503,

Fax: +381 21 475 0 572, dumnic@uns.ac.rs

Received: 29.12.2014 Accepted: 13.02.2015

Abstract- Indirect field oriented control (IFOC) of squirrel-cage induction generator (SCIG) with full capacity power converter used in wind energy conversion system (WECS) is presented in this paper. In order to improve WECS reliability robust IFOC algorithm using artificial intelligence (AI) for speed estimation was developed. Estimated speed is used for realization of maximum power tracking algorithm (MPPT). Practical testing and validation of considered estimation techniques is performed using advance laboratory prototype of WECS. Extensive experimentation is conducted in order to verify efficiency and reliability of proposed speed-sensorless control technique under realistic WECS operating conditions. The experimental results show the high level of performance obtained with the proposed speed-sensorless vector control method. Introduction of AI improved dynamics characteristics of WECS making proposed control method suitable for commercial application.

Keywords— Wind energy; Induction generator; Rotor speed estimation; MRAS algorithm; Artificial intelligence.

1. Introduction

Worldwide energy market currently exhibits constant and steady growth in energy demand. However, the increase in energy generation is currently accompanied by certain adverse effects on the environment. In that regard, humanity should look to implement a sustainable energy mix, with renewable energy sources (RES) providing quite a useful tool for this particular purpose. The share of energy generated from RES will exceed 25 % by 2035 worldwide, while wind would become a second largest sources making up a quarter of the total share of RES [1]. It still remains to be seen if the goal set by the European Union (EU) for 2020 will be achieved with 20% share of RES in total electrical energy generation. While EU-28 framework legislation and the targets for 2020 ensure a degree of stability in the development of renewable energy market, the share of EU-28 energy demand is only about 17 % of total worldwide energy generation. Similar goals, like in EU, have been set by the US, with a share of 22 % in worldwide energy market, since they have identified RES as a mean to overcome the present global economic crisis. Additionally, this can prove to be useful for the US, while it look to lessen the public concern regarding ecological issues. Nonetheless, the highest impact on global energy policy is expected from Asian and Pacific countries and their respective policies, since they hold 35 % of world energy market [2]. With the energy demand rising for the developing countries, and stricter requirements for environment protection in EU-28 and US, RES will surely follow the expected trend and maintain constant increase of their share in the global energy scenario.

Wind Energy Conversion Systems (WECS) showed a positive trend of rapid development during the last decade, consequently leading to an increase of its share in global energy generation. Recent reports show that at the end of the year 2013 cumulative power of installed WECS worldwide was over 318 GW [1]. During the year 2013, more than 35 GW of new wind power capacity was brought online, but

in comparison to 2012, where global installation exceeded 45 GW, a sharp decline is evident [1].Wind energy market forecast shows the trend of stabilization after the 2014, where annual market growth should be expected at 6-10 % until 2018. This will lead to cumulative market growth averaging at 12-14 % from 2015-2018, ending with global cumulative installed capacity just about 600 GW by the end of 2018 [1].

The evolution of technology has led to the development of different types of WECS that make use of variety of topologies with different type of electric generator [3, 4]. The variable speed WECS with full-capacity power converters offers a lot of advantages over other topologies and it is one of the main configurations in today's wind power industry. Squirrel-cage induction generators (SCIG) are widely employed in WECS where the rotor circuits are shorted internally and therefore not brought out for connection with external circuits [5, 6]. Main features of SCIG are that they prove to be very robust and relatively inexpensive, while having a low maintenance cost. In order to obtain fast dynamic responses vector control techniques of SCIG is employed. Vector control algorithm requires accurate rotor speed signal of induction generator to achieve decoupled control of machine torque and flux. Acquiring such signals requires the introduction of speed sensors, that are highly sensitive to heat and vibrations, require additional wiring work and maintenance. On the other hand, all components for WECS are required to be highly reliable due to harsh environmental conditions and poor accessibility for maintenance (especially in case of offshore installation). It is obvious that introduction of sensitive speed sensor leads to the reduction of WECS robustness and increase in regular and emergency maintenance costs. Reliability of the WECS can, therefore, be improved by eliminating the speed sensor, whilst reducing maintenance cost [7].

At the present time, speed sensor elimination becomes possible due to rapid development of digital signal processors (DSP), allowing for the use of modern SCIG states and output estimation algorithms. Research focus for the large number of experts in the last several decades has been the development of control strategies that would allow speed-sensorless drives to achieve dynamic performances identical to those of standard drives that include speed measurement. Low performance, or even average performance speed-sensorless SCIG drives prioritize simple speed estimation techniques, since they are relatively easy to implement. Most common speed estimation techniques in use are: open loop speed estimation, Model Reference Adaptive System (MRAS) and Sliding Mode Observer. Derating performance of such estimator can occur when there is inconsistency in the parameters between the model and the machine, current and voltage sensors inaccuracy, but also due to non-linear behavior of voltage source converter. This can particularly be underlined for the open loop estimation [8, 9]. Introduction of Artificial Intelligence (AI) to standard estimation techniques can improve their dynamic performance and steady state response. Moreover, known AI topologies show relative insensitivity to machine parameter variation adding to the robustness of the algorithm. Additionally, with the use of AI, complex mathematical model of the machine with speed dependency can be completely avoided.

Practical implementation of speed-sensorless vector controlled SCIG in variable speed WECS is presented in this paper. Speed estimation is implemented based on classical MRAS observer modified with Artificial Neural Network (ANN). ANN is fitted in the part of the MRAS observer, while weight coefficient is proportional to the machine speed. This paper presents the technical background for the SCIG vector control and ANN speed estimation and show the dynamic and steady state performance of the system. All results are experimentally validated using advanced laboratory setup. The speed estimation method proposed in this paper is capable of tracking the rotational speed not only in the steady state but also when the WECS is subject of fast dynamic changes. Proposed technique is computationally very efficient and easy to implement, which, in addition to its robustness, makes it suitable for utilization in WECS. Principal contributions is concise and precise presentation of the complete theoretical background and practical implementation of AI based vector control strategy, including detailed ANN design process, intended for the use in WECS.

2. Overview of System Topology and Control Strategy

2.1. System Topology with Full-Capacity Converter

Constant decrease in price for semiconductors with the improvement of reliability led to an increase in number of full-capacity power converters in WECS. The overview of WECS with full-capacity converters and SCIG is represented in Fig. 1. Topology for the full-capacity converter is back to back two-level voltage source converter (VSC). Both VSCs employ IGBTs as main switching components, are identical in topology and coupled using DC-link. Typical power rating of WECS with full-capacity converter is up to 0.75 MW at the 0.69 kV voltage level. In order to surpass the power limitation of standard VSC, parallelization of IGBT modules can be employed. Similar effect can be achieved by parallelizing several VSC channels [5]. To implement maximum power point tracking (MPPT) algorithms, the generator side converter (voltage source rectifier - VSR) is used to control machine speed and/or torque. Power transfer is completed by the grid side converter (voltage source inverter - VSI), controlling the DC-link voltage and injected active and/or reactive power. This allows for fully independent operation of SCIG in full speed range, while VSI fulfills all the necessary requirements regarding the grid synchronization. Since the focus of this paper is speed-sensorless vector control of SCIG, control of grid side converter is performed using standard control techniques and those will not be discussed in detail.

2.2. IFOC Strategy for Variable Speed SCIG

Field oriented control (FOC) is one of the most used control methods of modern AC drives systems [5, 10]. This method can be divided to Direct Field Oriented Control

(DFOC), Natural Field Oriented Control (NFOC) and Indirect Field Oriented Control (IFOC). The main difference between mentioned control techniques is in the method for obtaining the flux orientation (rotor flux angle).

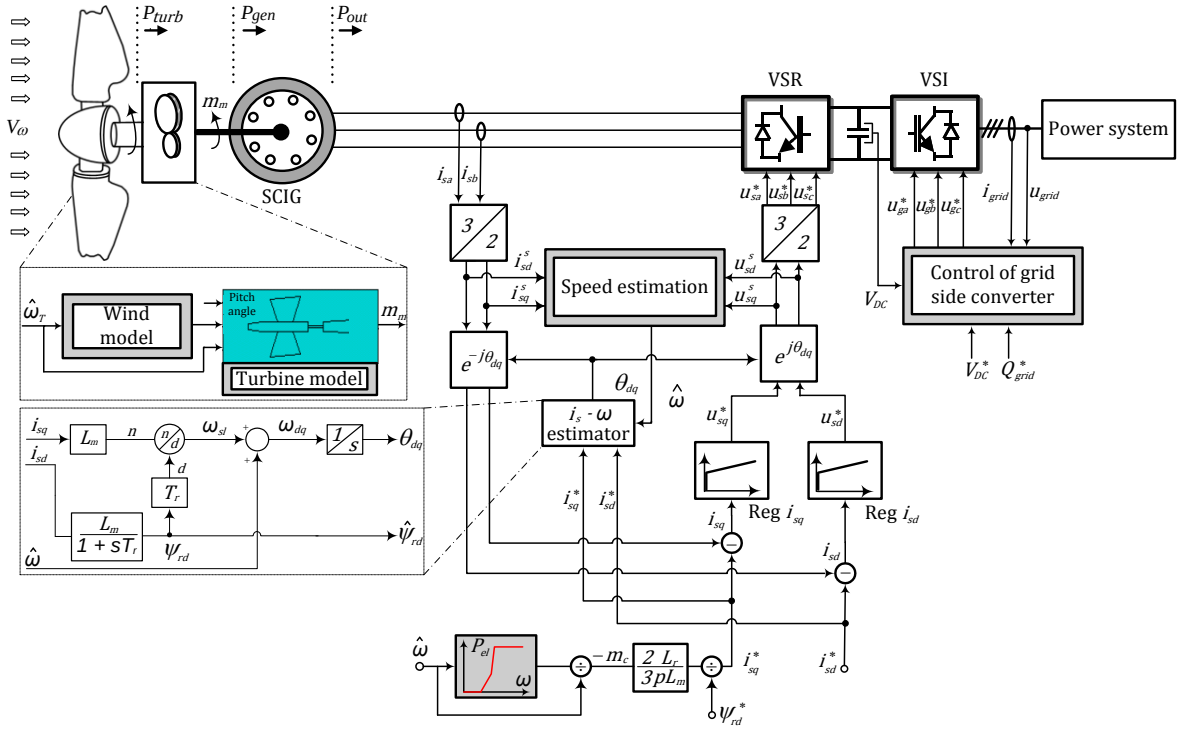

Fig. 1. Variable speed WECS with SCIG and full-capacity power converter.

Each of these methods provides certain advantages while having some drawbacks. The IFOC controlled drive can operate in four-quadrant down to standstill and it is widely used in both motor drives and power generating applications [11].

The rotor flux angle, for the IFOC control strategy can simply be acquired by the following equation:

$$\theta = \int (\omega + \omega_{sl}) dt \tag{1}$$

where ω_{sl} is the calculated slip frequency and ω is the SCIG rotor speed.

By aligning of the orthogonal synchronous reference frame with the rotor flux orientation, and by using well known decomposition techniques, actual rotor flux can be obtained as [5, 8]:

$$\psi_{rd} = \frac{L_m}{(1+sT_r)} i_{ds} \tag{2}$$

where rotor time constant is defined as $T_r = L_r / R_r$, L_r is rotor self-inductance and L_m is magnetizing inductance.

Usually, rotor flux reference is set to its rated value, while the decomposition allows for slip frequency calculation by using:

$$\omega_{sl} = \frac{L_m}{T_r \psi_{rd}} i_{qs} \tag{3}$$

According to SCIG rotor speed an MPPT algorithm generates a torque reference for the control of generator side converter. The reference for the q-axis controller can further be obtained by:

$$i_{qs}^* = \frac{2L_r}{3pL_m\psi_{rd}} m_c \tag{4}$$

Electromagnetic torque is thus controlled in q-axis by the q-axis current, while the d-axis controller sets the flux of the machine to the desired (nominal) value. If we assume constant flux, the SCIG torque becomes directly proportional to machine q-axis currents.

3. Algorithm for Estimation of SCIG Rotor Speed

Considering the environment of WECS during operation it is easy to understand severe conditions it has to endure. Unfavorable conditions can include wide temperature and wind speeds range, heavy torques, vibration and frequently even chemically aggressive environments (off-shore installations). Therefore, by eliminating speed sensor improvement in system robustness is achieved, with the additional benefit of significantly reducing regular and emergency services cost. In the recent decades, numerous techniques for induction machine (IM) rotor speed estimation have been developed. These techniques are solely based on machine currents and voltages measurement and are, therefore, used for speed estimation in shaft-sensorless drives. One of the most popular methods for induction machine rotor speed estimation is derived using Model Reference Adaptive System [8].

3.1. MRAS Algorithm

MRAS algorithm uses closed loop control system for estimation of rotor speed and can, therefore, be referred to as observer. Figure 2. presents three main components of the MRAS observer: reference model, adaptive model and adaptation mechanism. Reference model is a mathematical representation of the IM, having to faithfully reflect the current state of the machine.

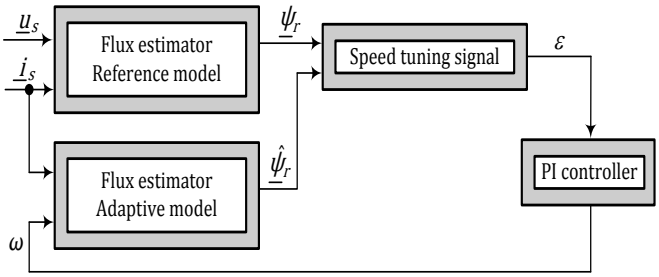

Fig. 2. MRAS based rotor speed observer.

This mathematical representation does not feature value estimated by MRAS observer, i.e. rotor speed. Adaptive model provides the insight in estimated value validity, since the mathematical representation include the estimated value of MRAS observer. Adaptation mechanism will, according to a predefined function, reach the estimated speed value using the difference between relevant values in reference and adaptive models. Common name for the reference model is voltage estimator, whereas adaptive mode is referred to as current estimator. MRAS observer based speed estimation can be classified according to the value selected for comparison between reference and adaptive model. Usually, rotor flux, stator flux, back EMF, active and reactive power are used [8]. This paper uses MRAS observer with relevant value for comparison chosen to be rotor flux. Rotor flux estimation is achieved using machine voltage equations for stator and rotor windings

Mathematical representation of reference model estimator is given by the Eq. (5). It is shown that this estimator uses stator voltages and currents to calculate rotor flux linkage components (ψ_{rd}, ψ_{rq}). Superscript (s) in these equations indicates that they are written in the stationary reference frame and L'_s is the stator transient inductance.

$$\psi^s_{rd} = L_r \Big/ L_m \left[\int \left(u^s_{sd} - R_s i^s_{sd} \right) dt - L'_s \, i^s_{sd} \right]$$
$$\psi^s_{rq} = L_r \Big/ L_m \left[\int \left(u^s_{sq} - R_s i^s_{sq} \right) dt - L'_s \, i^s_{sq} \right] \quad (5)$$

IM rotor voltage equations in stationary reference frame form adaptive model estimator given by the Eq. (6). Stator currents and speed signal is used for the calculation of rotor flux for this model. Symbol ^ in the following equations denote estimated quantities.

$$\hat{\psi}^s_{rd} = 1 \Big/ T_r \int \left(L_m i^s_{sd} - \hat{\psi}^s_{rd} - \hat{\omega} T_r \hat{\psi}^s_{rq} \right) dt$$
$$\hat{\psi}^s_{rq} = 1 \Big/ T_r \int \left(L_m i^s_{sq} - \hat{\psi}^s_{rq} + \hat{\omega} T_r \hat{\psi}^s_{rd} \right) dt \quad (6)$$

Rotor speed estimation is achieved using adaptation mechanism based on PI-type controller and is represented by the Eq. (7). Error value ε, according to the Eq. (8), is proportional to the sine value of angle difference between output vectors of reference and adaptive models. Using integral gain in adaptation mechanism it is ensured that the steady state value of ε is equal to zero.

$$\hat{\omega} = (K_p + \frac{K_i}{s}) \cdot \varepsilon \quad (7)$$

$$\varepsilon = \hat{\psi}^s_{rd} \psi^s_{rq} - \psi^s_{rd} \hat{\psi}^s_{rq} \quad (8)$$

Previously described MRAS observer has a complicated mathematical derivation, leading to model highly sensitive to induction machine parameter variation. In addition, the reference model is difficult to implement due to the pure integrators (Eq. (5)) which have problems with initial value and drift. To avoid this problem the output of the reference model must be connected to high-pass filter with the transfer function *s/(s+1/T)*. Since the reference model now gives modified rotor flux linkages, in front of the adaptive model the same high-pass filter block must be placed. The cut-off frequency of this filter is few Hertz. Below the cut-off frequency, the rotor speed estimation becomes inaccurate.

Furthermore, mentioned parameter variation between MRAS observer and the actual machine can be regarded as an encoder with an inherent ripple, which may lead to appearance of oscillatory behavior and, consequently, instability of the SCIG control. In addition, not only that dynamic performance of the SCIG will deteriorate, but it can also lead to a steady state error of the estimated speed [12]. Steady state error in generator speed estimation will have several adverse effects on the WECS performance [12, 13]. Namely, since the control algorithm uses speed signal for the MPPT, the system will not operate with maximum possible power. Additionally, both control algorithms for power limitation zone and pitch angle regulation system are going to exhibit faulty behavior, since they use speed as a control variable.

To improve the performance of the described MRAS observer, various practical techniques are also discussed which avoid the use of pure integrators. An AI based MRAS speed estimator seems to offer the most satisfactory performance. Introduction of a non-linear adaptive model with artificial neural network leads to an improvement in robustness of the control algorithm and, therefore, the complete drive, having significant increase in SCIG speed estimation precision. Moreover, the MRAS observer adaptation mechanism (PI controller) becomes unnecessary, since the integration is inherently made by the ANN based model in the adjustment mechanism [14].

3.2. Modified MRAS Algorithm Using Artificial Intelligence

Artificial neural networks can be categorized in several ways: e.g. into ANN that are trained and those that learn on their own (unsupervised or self-organized ANN). Classification based on structural complexity of the ANN leads to single-layer or multi-layer structures. For multi-layer feed forward neural network, containing hidden layers (one or several), supervised (off-line) training process, usually slow, has to be performed prior to ANN being used for real-time implementation. In contrast, this paper suggests the use of relatively simple two-layer ANN, that does not require a separate learning stage, while the learning is taking place during real-time rotor speed estimation process of SCIG. Presented ANN consists of input and output layer, with weight coefficients that can be adjustable or constant. Adjustable weight coefficient is directly proportional to rotor speed of SCIG. Error signal generated by the difference at the output of reference and adaptive model is used to alter adjustable weight. Fig. 3. represents the block diagram of speed estimation based on MRAS observer with two-layer ANN.

Weight coefficients of such ANN will be as following [14]:

$$w_1 = 1 - c \quad w_2 = \omega c T_r = \omega T \quad w_3 = c L_m \tag{9}$$

where c is defined as $c = T/T_r$, T is sampling time, and T_r is rotor time constant. Rotor time constant is adopted to have constant value, thus weight coefficients w_1 and w_3 are constant, while weight coefficient w_2 is proportional to the rotor speed.

Rotor flux linkages at the k-th sample can be derived from discrete representation of adaptive model in Eq. (6), using defined weight of two-layer ANN shown in Eq. (9), as:

$$\begin{aligned} \hat{\psi}^s_{rd}(k) &= w_1 \hat{\psi}^s_{rd}(k-1) - w_2 \hat{\psi}^s_{rq}(k-1) + w_3 i^s_{sd}(k-1) \\ \hat{\psi}^s_{rq}(k) &= w_1 \hat{\psi}^s_{rq}(k-1) + w_2 \hat{\psi}^s_{rd}(k-1) + w_3 i^s_{sq}(k-1) \end{aligned} \tag{10}$$

If we look to minimize mean square error (least mean square – LMS learning rule) of the rotor flux linkage estimation, weight coefficient w_2 has to be adjusted using the following adaptation mechanism:

$$\begin{aligned} w_2(k) = w_2(k-1) + \Delta w_2(k) = w_2(k-1) - \eta \cdot \\ \left\{ \left[\psi^s_{rd}(k) - \hat{\psi}^s_{rd}(k) \right] \hat{\psi}^s_{rq}(k-1) - \left[\psi^s_{rq}(k) - \hat{\psi}^s_{rq}(k) \right] \hat{\psi}^s_{rd}(k-1) \right\} \end{aligned} \tag{11}$$

where η is called learning rate, a positive constant value that affects the weight change dynamics. The LMS learning law leads to finite steady state value (assuming they converge), only when the weight adjustments are small. Since the correction depends on the error between estimated (adaptive model) and actual (reference model) rotor linkage flux, only a small portion of the error is used for adjustment of the weights in every calculation step. Thus the value of learning rate parameter needs to be $\eta << 1$ [15].

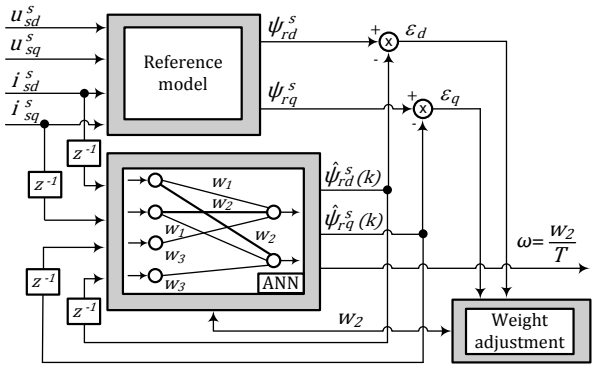

Fig. 3. Modified MRAS algorithm using two-layer ANN.

For the practical implementation, learning rate is sought to be as high as possible, consequently aiming for fastest possible ANN responses. On the other hand, a value too high will lead to the oscillations at the ANN output. In order to accelerate the convergence, without undesired effects on the ANN output adjustable weight coefficient is improved by addition of momentum term (inertia), achieving reliable and efficient learning. Therefore, calculated weight coefficient for the k-th sampling instant ($\Delta w_2(k)$) is supplemented with fraction of most recent coefficient adjustment ($\Delta w_2(k-1)$), making the adaptation mechanism become:

$$\begin{aligned} w_2(k) &= w_2(k-1) + \Delta w_2(k) + \alpha \Delta w_2(k-1) \\ &= w_2(k-1) + \eta \left\{ -\left[\psi^s_{rd}(k) - \hat{\psi}^s_{rd}(k) \right] \hat{\psi}^s_{rq}(k-1) \right. \\ &\left. + \left[\psi^s_{rq}(k) - \hat{\psi}^s_{rq}(k) \right] \hat{\psi}^s_{rd}(k-1) \right\} + \alpha \Delta w_2(k-1) \end{aligned} \tag{12}$$

The supplement ($\alpha \Delta w_2(k-1)$) is called the momentum term. Parameter α is a user-selected positive constant called the momentum constant with value typically ranging from 0.1 to 0.8 [16]. Finally, considering previously described structures of MRAS algorithm using ANN, it is possible to estimate rotor speed of SCIG with the following:

$$\begin{aligned} \hat{\omega}(k) &= \hat{\omega}(k-1) + \Delta w_2(k)/T + (\alpha/T)\Delta w_2(k-1) = \\ &= \hat{\omega}(k-1) + \eta \left\{ -\left[\psi^s_{rd}(k) - \hat{\psi}^s_{rd}(k) \right] \hat{\psi}^s_{rq}(k-1) + \right. \\ &\left. \left[\psi^s_{rq}(k) - \hat{\psi}^s_{rq}(k) \right] \hat{\psi}^s_{rd}(k-1) \right\} / T + (\alpha/T)\Delta w_2(k-1) \end{aligned} \tag{13}$$

4. Experimental Validation of the Proposed WECS Sensorless Control Scheme

4.1. Description of Laboratory WECS Prototype

Proposed speed-sensorless control strategy for variable speed WECS with full-capacity converter is tested and verified using advanced laboratory prototype for control of electrical drives and power electronic converters [17]. This advance R&D station is developed by authors of this paper and it is capable of running different type of complex and demanding control strategies for three-phase systems (with bidirectional power flow), as well as for multi- phase systems (five-phase or six-phase). For experimental validation of previously presented theory, the setup was

organized to operate as a small scale variable speed WECS. Overview of the experimental setup is shown in Fig. 4.

Control algorithms are implemented using highly modular and versatile dSPACE control hardware [18]. In Fig. 4 control hardware designated by ① executes IFOC strategy, speed estimation and MPPT algorithm for the control of generator side converter designated by ②. Control of grid side converter ③, coupled by the DC-link with generator side converter, is implemented using standard techniques and will not be further discussed since it is not the focus of this paper. In addition, dSPACE also generates the reference for wind turbine emulator, consisting of power converter ④ and torque controlled machine. Torque controlled machine is mechanically coupled with the SCIG and the coupled group is marked by ⑤.

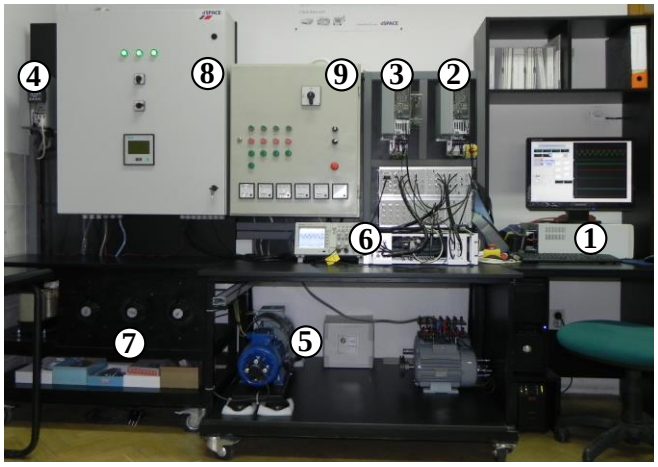

Fig. 4. Small scale WECS laboratory prototype.

Data acquisition, control signals and measured signals are routed through adapter block indicated by ⑥. A power transformer ⑦ represents the point of common coupling where the generated power is supplied to the distribution network. Two distribution cabinet designated by ⑧ and ⑨ hold switching, protection and control gear.

4.2. Control Algorithm Organization and Implementation

Control algorithm is organized according to the proposed theory and block diagram shown in Fig. 1, with full visual block oriented programming in Matlab/Simulink software tool. Real-time experimentation process is done by Control-Desk software, while the linking is performed by Real Time Interface (RTI) tools [18].

Control algorithm for real-time implementation, presented in Fig. 5., is implemented in several subsystems with different execution rate. The subsystem containing measurements (SCIG currents and DC-link voltage), software system protection and PWM generation is executed at 8 kHz sampling frequency triggered by the interrupt at the midpoint of PWM period. In theory, IFOC algorithm should be executed at least two times slower than PWM generation, leading to 4 kHz execution rate for current control and speed estimation subsystem. Faster subsystem generates the trigger by down-sampling of the basic trigger. Correspondingly, MPPT algorithm is achieved in the last subsystem at 1 kHz, since the time constant of the WECS mechanical subsystem is significantly higher and faster control would be ineffective.

Variable speed WECS control algorithm is based on minimum number of sensors with just two currents and one DC-link voltage sensor. Required SCIG stator voltages are reconstructed based on an array of PWM impulses generated by the digital controller. Adverse effects like voltage drop on semiconductors, finite switching time for semiconductors and the dead time can cause the difference between actual and reconstructed stator voltage value. However, considering the finite WECS speed operating ranges, this deviation, which is especially high for low speed IM operating zone, for this particular application is irrelevant.

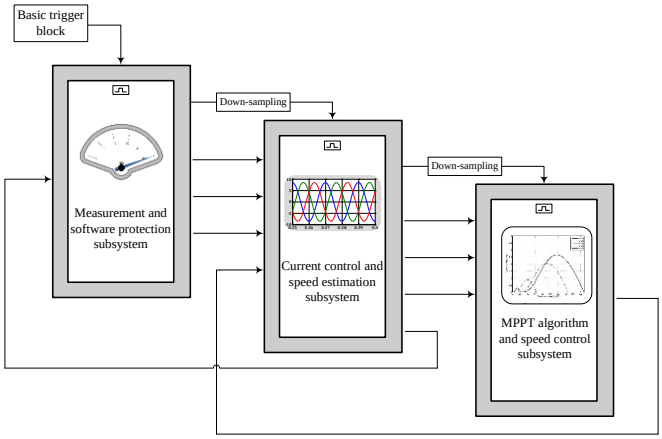

Fig. 5. Structural organization of the control algorithm for real-time implementation.

4.3. Experimental Results

Using previously described prototype, proposed control algorithms for variable speed WECS without speed sensor has been implemented. At first, in order to validate speed estimation techniques, the proposed algorithms have been tested in speed control mode. Therefore, speed closed loop IFOC strategy for IM is implemented with encoder obtained speed signal. Speed measurement is used to appropriately compare proposed speed estimation technique. Figure 6 shows the estimated speed response of IM using standard MRAS observer. Speed reference, in this experiment, is set to 0 [rpm] until 3.9 [s], when reference value changed to 1000 [rpm] with soft start slope of 625 [rpm/s]. As a consequence of introducing high-pass filter blocks, described in chapter 3.1. the standard MRAS observer has inaccurate speed estimation at zero speed. Tracking of the IM rotor speed, after high-pass filter cut-off frequency, shows fast response and satisfactory dynamic characteristics. However, it can be noted that estimated speed from standard MRAS observer has high content of noise (undesired high-frequency spectrum component), mainly introduced and enhanced by the PI controllers in adaptation mechanism. This can lead to oscillatory behavior and instability of the algorithm especially if other adverse effect like machine parameter detuning is considered. One possible approach to overcoming this is to introduce a filtering of the signal at the

output of standard MRAS observer. Signal filtering will damp unwanted components of the signal but will introduced the delay in estimated speed signal. This will lead to WECS control system to being misaligned whit the actual rotor position, thus causing the reduction in energy generation.

Similar set of experiment is performed to validate the improvement of MRAS observer with ANN based adaptive model. ANN has been implemented according to proposed theory, with learning coefficient chosen to be η = 0.009 and the momentum term α = 0.65, according to [14, 16]. Speed reference, in this experiment, is set to 0 [rpm] until 4.3 [s], when reference value changed to 1000 [rpm] with soft start slope of 2000 [rpm/s]. Steeper soft start slope was selected to demonstrate dynamic capability of ANN based MRAS observer. Figure 7a shows the estimated speed response of IM using MRAS observer with ANN for given set of parameters. Proposed technique obviously leads the estimated signal to a finite steady state response, but the noise and oscillations make this signal unacceptable. As proposed by the theoretical discussion, to lessen the adverse effect learning coefficient should be η << 1. By manual tuning of the parameter, optimal learning coefficient is found to be η = 0.00009, while keeping the momentum term at the same value. Increment of the adjustable weight coefficient (w_2) clearly represents the influence of the learning coefficient on the ANN speed response which is also visible in Fig. 7. Clearly, MRAS observer based on ANN has the most suitable steady state and dynamic response characteristics, as proven by Fig. 7b.

After successfully implementation of speed estimation technique using ANN based MRAS observer, the laboratory prototype is reconfigured to operate as a variable speed-sensorless WECS. Machine emulating WECS mechanical part produces torque equivalent to wind power at average speed of 11.5 [m/s] and turbulence intensity of 12 %. Torque reference has been generated using an adequate tool from Wind Turbine Blockset for Matlab/Simulink based on the actual wind measured data from a perspective WECS location [19].

Machine current waveform and estimated fluxes value in stationary reference frame are given in Fig. 8a and 8b, respectively. As one validation of successful implementation of variable speed WECS speed-sensorless IFOC control, observed currents are sinusoidal, while the fluxes make an ideal circular shape.

Figure 9a represents torque reference for the machine emulating wind turbine. SCIG currents in synchronous rotating reference frame are shown in the Fig. 9b. Clearly, the q-axis current component follows the turbine torque showing that the MPPT algorithm is implemented successfully. Furthermore, IFOC strategy is properly applied since decoupled control has been achieved between d and q-axis current components. Estimated SCIG speed signal used for MPPT and generation of q-axis current reference value is given in Fig. 9c. It can be concluded that ANN based MRAS estimated speed match the speed signal obtained from encoder under proposed WECS realistic conditions.

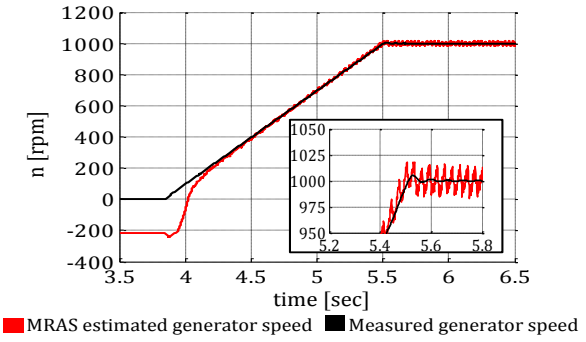

Fig. 6. Experimental validation of MRAS observer – speed response.

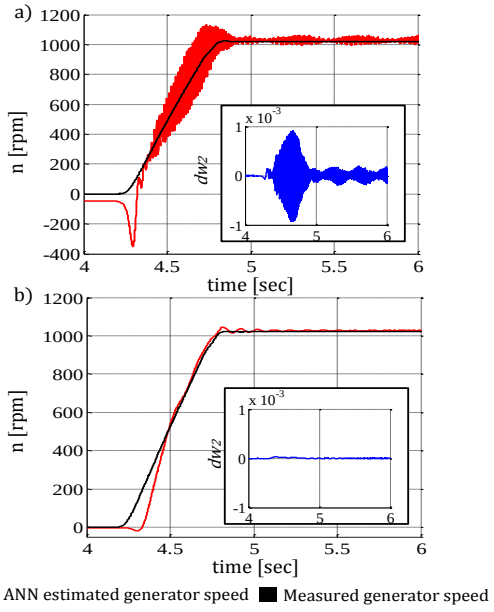

Fig. 7. Experimental validation of ANN based MRAS observer – speed response with learning coefficient η = 0.009 (a) and η = 0.00009 (b).

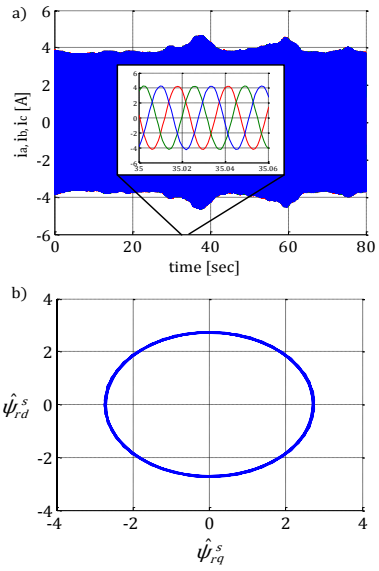

Fig. 8. SCIG currents in time domain (a) and ANN estimated rotor flux linkages (b). for laboratory speed-sensorless WECS prototype experiment.

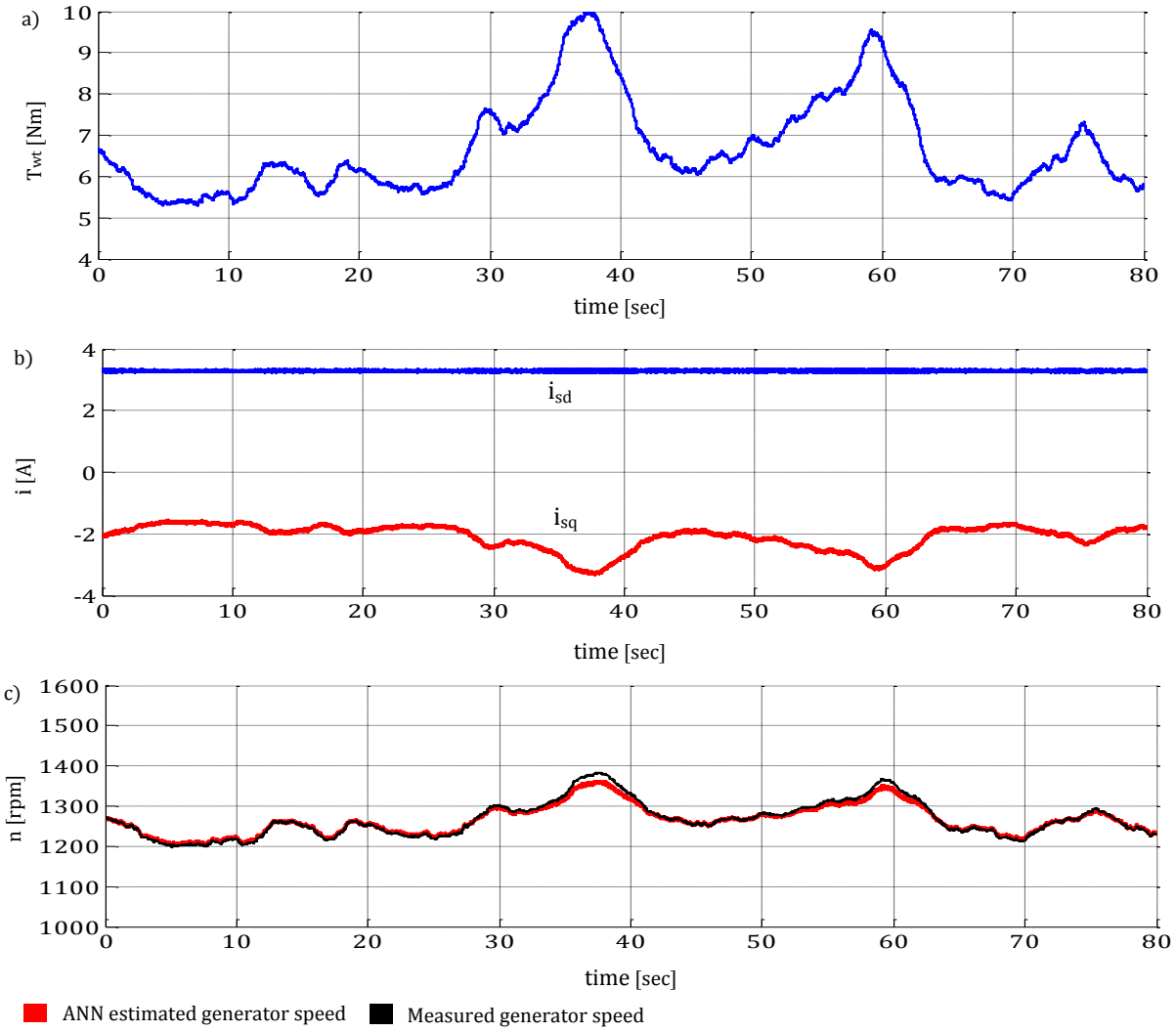

Fig. 9. Torque reference of wind turbine emulator (a), SCIG currents (b) and rotor speed signals (c) for laboratory speed-sensorless WECS prototype experiment.

5. Conclusion

This paper presents implementation of IFOC algorithms for variable speed-sensorless WECS with SCIG rotor speed estimation using ANN based MRAS observer. Fundamental theoretical considerations for IFOC and popular speed estimation technique (MRAS observer) are given. Main deficiency of standard MRAS estimation algorithm for the use in WECS is theoretically exposed and experimentally validated. In respect, benefits of introducing artificial intelligence to standard estimation technique are analyzed. The paper discuses replacement of MRAS adaptive model with simple two-layer ANN which does not require a separate learning stage. Proposed speed estimation technique has satisfactory dynamics and steady-state response. The influence of the ANN learning coefficient on system response oscillation and stability is shown to be high. With optimally selected ANN parameters accurate speed estimation and stable operation of variable speed WECS is achieved. This is experimentally verified on laboratory prototype of WECS under the realistic conditions. High precision matching of the SCIG estimated and actual speed makes it possible to implement high performance vector controlled WECS with MPPT. Developed control strategy, with clear improvement of the dynamics characteristics, leads to novel applicable solution for reliable and robust WECS, with reduced overall cost.

Acknowledgements

This paper is a result of the scientific project No. III 042004 of Integrated and Interdisciplinary Research entitled "Smart Electricity Distribution Grids Based on Distribution Management System and Distributed Generation", funded by Republic of Serbia, Ministry of Education and Science.

References

[1] GWEC Report, Global Wind Report – Annual market update 2013, *Global Wind Energy Council*, 2013.

[2] A. Belhamadia, M. Mansor, M. A. Younis, "A Study on Wind and Solar Energy Potentials in Malaysia", *International Journal of Renewable Energy Research – IJRER*, Vol.4, No.4, pp. 1042-1048, 2014.

[3] N. S. Patil, Y. N. Bhosle, "A Review On Wind Turbine Generator Topologies", *International Conference on Power, Energy and Control (ICPEC)*, pp.625-629, 6-8 Feb. 2013. doi: 10.1109/ICPEC.2013.6527733

[4] A. G. Aissaoui, A. Tahour, M. Abid, N. Essounbouli, F. Nollet, M. I. Chergu, "Variable Structure Control Applied in Wind Turbine Based on Induction Generator", *International Journal of Renewable Energy Research – IJRER*, Vol.2, No.4, pp. 600-607, 2012.

[5] B. Wu, Y. Lang, N. Zagari, S. Kouro, *Power Conversion and Control of Wind Energy Systems*, John Wiley and Sons, IEEE Press, USA, 2011, ch. 5, ch. 7.

[6] R. Teodorescu, M. Liserre, P. Rodriguez *Grid Converters for Photovoltaic and Wind Power Systems*, John Wiley and Sons, IEEE Press, USA, 2011, ch. 6.

[7] J. B. Alaya, A. Khedher, M. F. Mimouni, "Speed-Sensorless DFIG Wind Drive Based on DTC Using Sliding Mode Rotor Flux Observer", *International Journal of Renewable Energy Research –IJRER*, Vol.2, No.4, pp. 736-745, 2012.

[8] P. Vas, *Sensorless Vector and Direct Torque Control*, Oxford Univ. Press, NY, 1998, ch. 4.

[9] M. Hinkkanen, J. Luomi, "Parameter sensitivity of full-order flux observers for induction motors", *IEEE Transactions on Industry Applications*, vol.39, no.4, pp.1127-1135, July-Aug. 2003.

[10] J.A. Santisteban, R.M. Stephan, "Vector control methods for induction machines: an overview", *IEEE Transactions on Education*, vol.44, no.2, pp.170-175, May 2001.

[11] F. Blaabjerg F. Iov, T. Kerekes, R. Teodorescu, "Trends in Power Electronics and Control of Renewable Energy Systems", *14th International Conference of Power Electronics and Motion Control*, K1-K19, EPE-PEMC 2010.

[12] M. Wang, E. Levi, "Evaluation of Steady-State and Transient Behavior of a MRAS Based Sensorless Rotor Flux Oriented Induction Machine in the Presence of Parameter Detuning", *Electric Machines and Power Systems*, Vol. 27, no. 11, pp. 1171 – 1190, 1999.

[13] B. Dumnic, V. Katic, V. Vasic, D. Milicevic, M. Delimar, "An Improved MRAS Based Sensorless Vector Control Method for Wind Power Generator" *Journal of Applied Research and Technology – JART*, Vol. 10. no. 5, pp. 687-697, October 2012.

[14] P. Vas, *Artificial-Intelligence-based Electrical Machines and Drives: Application of Fuzzy, Neural, Fuzzy-neural, and Genetic-algorithm-based Techniques*, Oxford University Press, 1999, ch. 5.

[15] B. Yegnanarayana, *Artificial Neural Networks*, Prentice-Hall of India, New Delhi, 2005, ch. 1.

[16] J. M. Zaruda, *Introduction to Artificial Neural Systems*, Jaico Publishing House, 2005, ch. 4.

[17] B. Dumnic, D. Milicevic, B. Popadic, V. Katic, Z. Corba, "Advanced laboratory setup for control of electrical drives as an educational and developmental tool", *EUROCON*, pp. 903-909, Zagreb, Croatia, July 2013.

[18] dSpace manual, Modular Systems – Hardware Installation and Configuration Reference, *dSpace gmbh*, 2014.

[19] F. Iov, A. D. Hansen, P. Sorensen, F. Blaabjerg "Wind Turbine Blockset in Matlab/Simulink," UNI. PRINT Aalborg University, March 2004.